

# Frequency Agile Solar Radiotelescope

*A Next Generation Radio Telescope for Solar  
Astrophysics and Space Weather*

T. Bastian (NRAO)	J. Qiu (U Montana)
H. Bain (NOAA)	K. Reeves (SAO/CfA)
R. Bradley (NRAO)	P. Saint-Hilaire (UCB/SSL)
B. Chen (NJIT)	S. Schonfeld (NMSU)
J. Dahlin (GSFC)	Chengcai Shen (SAO/CfA)
E. DeLuca (CfA)	S. Tun (NRL)
J. Drake (U Maryland)	D. Wertheimer (UCB/RAL)
G. Fleishman (NJIT)	S. White (AFRL)
D. Gary (NJIT)	
L. Gleasoner (U Minn)	
Fan Guo (LANL)	
G. Hallinan (Caltech)	
G. Hurford (UCB/SSL)	
J. Kasper (U Mich)	
Hantao Ji (Princeton)	
J. Klimchuk (NRL)	
A. Kobelski (WVU)	
S. Krucker (UCB/SSL)	
N. Kuroda (NRL)	
D. Longcope (U Montana)	
C. Lonsdale (MIT)	
J. McTiernan (UCB/SSL)	
G. Nita (NJIT)	

**A white paper submitted to the  
Astro2020 Decadal Survey**

# 1 Introduction

Solar activity represents a uniquely accessible example of the ubiquitous processes of energy release and particle acceleration that occur in a wide range of contexts, from planetary magnetospheres to the galaxy. Among multi-wavelength observations of solar phenomena, radio observations provide a unifying perspective because of their sensitivity to both thermal plasma and nonthermal particles and their unique sensitivity to solar magnetic fields—the energy source for solar activity. Radio emission is particularly unsurpassed in its sensitivity to accelerated particles. The spatially-resolved radio spectrum provides a powerful source of diagnostic information with the potential for transformational insights into solar activity and its terrestrial impacts. The same processes that convert magnetic energy to accelerated particles during solar activity occur in many other astrophysical contexts, and what we learn of these processes from solar radio studies is directly applicable to them.

The need to develop the necessary ground based observational infrastructure and analysis tools to exploit radio observations of the Sun has long been recognized. The *Frequency Agile Solar Radiotelescope* (FASR) meets this need. FASR is a solar-dedicated radio telescope (a radioheliograph) designed to fully exploit the potential of radio diagnostics, combining superior imaging capability and ultra-broad frequency coverage to address a wide range of science goals.

The potential value of FASR to the solar, heliophysics, and space weather science communities – as well as the astronomy and astrophysics community - has been recognized by *four* (!) previous decadal surveys, two in *Astronomy and Astrophysics* [22,24] and two in *Solar and Space Physics*. [23,25] Specifically, it was ranked as the number one ground-based project by the *Solar and Space Physics* decadal, while the Astro2010 decadal radio-millimeter-submillimeter panel ranked FASR second, behind HERA. Astro2010 performed a CATE analysis of FASR, described it as “doable now” and singled it out as an exemplar of an ideal mid-scale program. While NSF has now developed a mid-scale infrastructure budget line, it was only this year that it became available as an agency-wide “big idea”. Therefore, no investments in FASR development have been made during the past decade with one outstanding exception: the FASR concept has been validated by the *Expanded Owens Valley Solar Array* (EOVSA), a 13-antenna pathfinder array deployed by NJIT at the Owens Valley in California, funded by an NSF MRI-R2 grant, that leveraged previous FASR design work. Some important EOVSAs results are discussed in the next section.

This white paper outlines steps necessary to restart the FASR initiative to bring this unique and powerful instrument to fruition.

## 2 FASR Science Goals and Objectives

FASR is a radio interferometric array designed to perform Fourier synthesis imaging. FASR is a specialized instrument – one designed and optimized for high-fidelity spectral analysis over the extreme range of flux density and timescales presented by the Sun. Yet FASR science is as broad as solar physics itself. The major advances offered by FASR over previous generations of solar radio instruments are its unique combination of **ultra-wide frequency coverage, high spectral and time resolution, and excellent image quality**. FASR measures the polarized brightness temperature spectrum along every line of sight to the Sun as a function of time. The concept

proposed here would operate from 200 MHz to 20 GHz, while low frequencies would be covered by the already funded upgrade to the Long Wavelength Array at the Owens Valley Radio Observatory (OVRO-LWA). Radiation over this vast wavelength range probes the solar atmosphere from the middle chromosphere to several solar radii into the corona, a dynamic, magnetoactive, plasma environment in which a wealth of astrophysical processes occurs. FASR images the entire solar atmosphere several times a second from the chromosphere through the corona, while retaining the capability to image a selected frequency range with as little as 20 ms time resolution. Moreover, FASR's panoramic view allows the solar atmosphere and the physical phenomena therein, both thermal and nonthermal, to be studied as a coupled system.

Here we summarize several science goals of the proposed instrument while at the same time emphasizing the fundamentally new observables enabled by FASR. With its unique and innovative capabilities FASR also has tremendous potential for new discoveries beyond those presently anticipated. The science objectives described below flow down to science requirements as summarized in matrix given in Table 1.

## 2.1 Leading Science Objectives

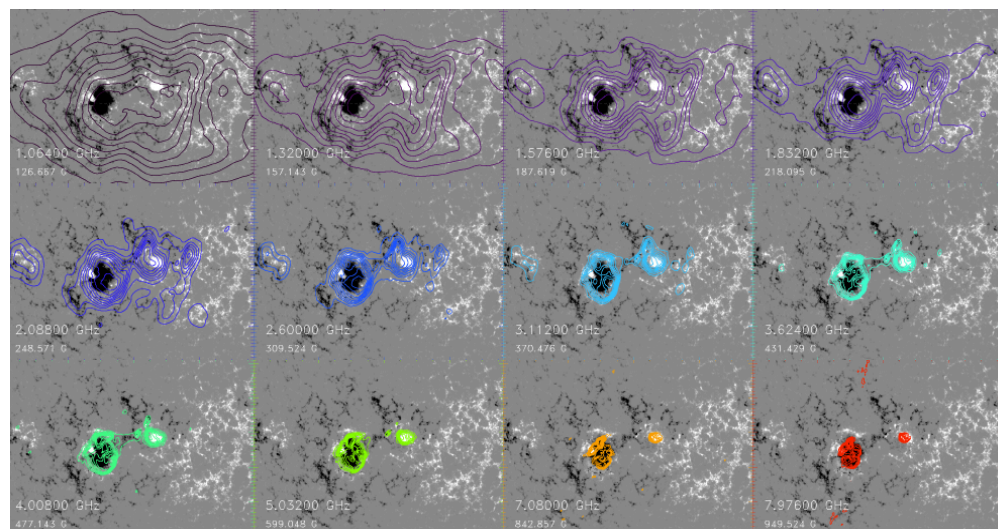
### 2.1.1 *The Nature and Evolution of Coronal Magnetic Fields*

Quantitative knowledge of coronal magnetic fields is fundamental to understanding essentially all solar phenomena above the photosphere, including the structure and evolution of solar active regions, magnetic energy release, charged particle acceleration, flares, coronal mass ejections (CMEs), coronal heating, the solar wind and, ultimately, space weather and its impact on Earth. Characterized as the solar and space physics community's "dark energy" problem [20], useful quantitative measurements of the coronal magnetic field had been largely unavailable until recently. Although understood in principle for many years, available instrumentation has not been available in practice to exploit radio observations to make quantitative measurements of coronal magnetic fields. This has recently changed, with breakthrough flare observations by the FASR pathfinder EOVS [e.g., 16] and broadband observations of solar magnetic active regions by the Karl G. Jansky Very Large Array (JVLA; Fig 1) which demonstrate the use of radio observations for measuring the strength and dynamics of coronal magnetic fields. These efforts are complementary to numerical extrapolations of measurements of the magnetic field distribution at the photospheric or chromospheric level [11], as well as on-going efforts at O/IR wavelengths to make measurements of above-the-limb coronal magnetic fields via the Hanle and Zeeman effects (e.g., with DKIST and COSMO). Yet these current efforts are far from what is possible and what is needed for scientific progress.

The FASR approach is **the only means currently available to measure coronal fields against the solar disk** as well as above the limb. This is an essential feature for comparison with photospheric extrapolations, because accurate extrapolations are not possible above the limb, where the photospheric measurements are not available. A striking example is provided by radio observations of thermal gyroresonance emission [6,34,35 – see also the White Paper by Fleishman et al. 2019]. In the presence of magnetic fields greater than  $\sim 100$  G, such as those present in solar active regions, the corona becomes optically thick to absorption at low harmonics of the electron gyrofrequency  $\nu_e = 2.8 sB$  MHz, where  $s$  is the harmonic number (typically  $s = 2, 3$  for coronal conditions) and  $B$  is the magnetic field in Gauss. By imaging across a broad range of frequencies

(approximately 1.5–20 GHz), the thin isogauss resonance layer varies systematically with height, allowing a CAT-scan-like view of nested layers up to coronal magnetic field strengths as high as 1800 G [7], embodying 3D information about the coronal magnetic field. This stands in stark contrast to the mean longitudinal magnetic field measured using the Zeeman effect, for example, using optically thin line emission at O/IR wavelengths. Fig. 1 shows an example of a JVLA observation from 1-8 GHz that shows the coronal isogauss surfaces above an active region (AR 12209) from  $\sim 125$  G to 950 G. Several additional radio techniques, detailed by [14], are available for measuring coronal magnetic fields in a wide variety of physical environments ranging from the quiet solar atmosphere to dynamic phenomena like solar flares and coronal mass ejections. While the non-solar-dedicated JVLA can do this on an occasional (proposal-driven) basis, and EOVSAs can make daily crude measurements, only FASR can fully exploit this revolutionary capability with high fidelity, high resolution spectropolarimetry.

**Fig. 1** An example of gyroresonance emission above a large solar active region in November 2014. Contours show isogauss surfaces. Coronal magnetic fields of 140-980G are sampled.



### 2.1.2 The Physics of Flares

Outstanding problems in the physics of flares include those of magnetic energy release [12], particle acceleration, and particle transport. As flare energy release requires the participation of a large coronal volume sometimes comparable to the size of the entire active region [31] one of the key challenges lies in the lack of measurements for key physical parameters in a broad region around the flare energy release site. At centimeter wavelengths, gyrosynchrotron emission – radiation from nonthermal electrons with energies of 10s of keV to several MeV gyrating in a magnetic field – illuminates any magnetic coronal loop to which energetic electrons have access, showing when and where accelerated electrons are present. Inversion of the gyrosynchrotron spectrum allows **both the magnetic field in the flaring source and the electron energy distribution** to be deduced, as well as their spatiotemporal evolution. EOVSAs has recently demonstrated the power and utility of broadband (2.5–18 GHz) imaging spectropolarimetry with observations of the celebrated flares of September 2017 [e.g., 29]. EOVSAs measures both the dynamically changing magnetic field strength and connectivity of the erupting source (e.g. Fig. 2), otherwise invisible at other wavelengths, but also the spatially and temporally evolving electron distribution function, placing new constraints on the magnetic energy release in the flaring source and on electron acceleration [13,15 and the White Paper by Gary et al. 2019]. Perhaps equally importantly, imaging spectroscopy from EOVSAs reveals that microwave emission is present over

a much wider area around the magnetic energy release site than previously expected (Fig. 2; from [29]), which opens up the potential for measuring the aforementioned critical physical parameters not only limited to the primary site where most microwave-emitting accelerated electrons are present, but also from a much broader region where the magnetic energy release and particle acceleration and transport processes occur.

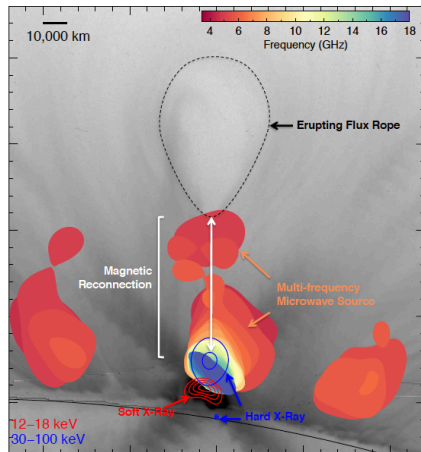


**Fig. 2** EOVSAs observation of the 2017 September 10 X8.2-class flare. *Greyscale*: The event was associated with the eruption of a magnetic flux rope, which induced magnetic reconnection in an elongated current sheet. *Contours*: Nonthermal hard X-ray emission is seen at both the looptop and footpoint location (purple). Thermal X-ray emission is seen in post-flare loops (red contours). *Filled contours*: EOVSAs multi-frequency imaging data reveal the presence of energetic electrons (100s of keV) throughout the entire reconnection region and more distant outliers, invisible to any other current instrumentation. The color bar shows the corresponding frequency. See [15]. FASRs lower-frequency coverage would allow measurements to extend into the all-important flux-rope/cavity region (dashed line).

However, the limited dynamic range brought about by EOVSAs sparse array of 13 antennas (typically a few times 10:1) prevents the precise measurements from the microwave spectra outside the immediate site of the dominant microwave emission. Higher dynamic range and image fidelity are also required for investigating such important phenomena as non-power-law, broken power-law, and pitch angle dependence of the charged particle distribution, which are not possible with EOVSAs. FASRs superior imaging in this frequency range (2–20 GHz) is expected to improve the image dynamic range of EOVSAs by more than two orders of magnitude (to  $10^4$ :1), offering a revolutionary view of flare energy release and particle acceleration. Likewise, the extended frequency range of FASRs toward the lower frequency end (0.2–2 GHz) would allow tracking the charged particles into and above the erupting magnetic flux rope shown by the dashed contour in Fig. 2, and hence would allow measurements of similar physical parameters in this essential, but largely unexplored region downstream and upstream of the coronal shock ahead of the erupting flux rope, where the interplay between flare- and shock-driven particle acceleration is suspected to occur for the production of solar energetic particles (SEPs; [27]) and their space weather impacts.

We note that, in the coming decade, no NASA missions are currently in the planning stages that will provide HXR/g-ray imaging of nonthermal emissions from electrons  $>100$  keV. The stalwart *Ramaty High Energy Solar Spectroscopic Imager* (RHESSI) mission ended after 16 yrs in 2018. The only planned missions by other space agencies (ESA’s Solar Orbiter and China’s ASO-S) will be limited in flares observed due to data downlink limitations. Hence FASRs could be the **only consistently-available high-energy nonthermal imager available** for the next solar cycle.

FASRs extension toward lower frequencies (0.2–20 GHz) also provides access to plasma diagnostics that are unavailable at higher frequencies. For example, coherent spike bursts and type III bursts driven by electron beams accompany energetic phenomena such as solar flares [1]. They are intimately related to the energy release process [2,5] associated with magnetic reconnection in

both the impulsive phase of flares, and in post-flare loops [5]. The high frequency and time resolution of the JVLA has been used to demonstrate that the trajectories of electron beams can be traced from the magnetic reconnection site in X-ray jets and flares [8,10]. A spectacular example of the unique power of radio imaging spectroscopy at decimeter wavelengths, again by the JVLA, demonstrates the use of coherent radio emission to trace out the termination shock created by reconnection outflows resulting from magnetic energy release in a flare and to gain insight into its role in particle acceleration [9]. By imaging these phenomena simultaneously in different spectral regimes, FASR provides a unique and unprecedented view of coupled flare processes. Additional details are provided in the White Paper by Chen et al. (2019).

### 2.1.3 Drivers of Space Weather

The term “space weather” refers to phenomena that disturb the interplanetary medium and/or affect the Earth and near-Earth environment [18]. This includes recurrent structures in the solar wind (fast solar wind streams, co-rotating interaction regions), the ionizing radiation and hard particle radiations from flares, coronal mass ejections, and shock-accelerated particles. Each of these can cause phenomena on Earth that have societal impacts. The **science of space weather** (see the White Paper by Bastian et al. 2019a) is in a fledgling state but its relevance to modern society is highlighted by the OSTP’s *National Space Weather Strategy and Action Plan* (2019). Moreover, its relevance as a **touchstone for exo-space weather and planet habitability** is increasingly being recognized (see White Papers by Osten et al 2019 and Airapetian et al 2019), as well as to human deep space exploration. Comprehensive and diverse observations are needed to understand space weather as a complex system. The drivers of space weather are all solar in origin. FASR will be sensitive to eruptive flares, CMEs, filament/prominence eruptions, and type II (shock-driven) radio bursts. Interest in CMEs is particularly strong because they are associated with the largest geoeffective events and the largest solar energetic particle (SEP) events. With the detection of gyrosynchrotron radiation from CMEs at decimeter/meter wavelengths [3,21] a unique tool has become available to diagnose CME magnetic fields, critical to understanding their geoeffectiveness. With its unique ability to perform broadband imaging spectropolarimetry, **FASR will be able to simultaneously image the basic shock driver (flare or CME signature), the response of the atmosphere to the driver (chromospheric/coronal waves [35] and coronal dimming), and the shocks themselves** as a system. In doing so FASR will yield unique new insights into the relationship between flares, CMEs, SEPs and their space weather impacts.

### 2.1.4 Energetics of the Quiet Solar Atmosphere

The heating of the solar chromosphere and corona remains an enduring problem. Radio emission from the quiet Sun atmosphere is dominated by thermal free-free emission but nonthermal processes also play a role (e.g., [30]). At its highest frequency FASR will image the middle chromosphere and, as such will complement ALMA’s observations of the low chromosphere with similar angular resolution. By systematically tuning to lower frequencies, the height from which the (optically thick) emission originates moves through the top of the chromosphere and into the corona, again providing a 3D probe into the temperature, density, and the magnetic field structure [28] of the solar atmosphere. Resonant wave heating [e.g., 32] represents an important class of models for coronal heating and makes specific predictions of the location and time scales of energy deposition. Using free-free diagnostics, FASR observations of the resulting temperature changes in this region encompassing both the chromosphere and the adjacent corona can address the validity of such predictions. The role of “nanoflares” [17,36] in the energetics of the lower

atmosphere is also under active investigation. The energetics of such small events depends critically on their thermal properties and the role of accelerated electrons [30]. Again, the combination of FASR's frequency coverage and imaging can apply diagnostics to quantitatively address both thermal/nonthermal contributions of such events to the energy budget. A third important quiet Sun FASR science use case is to constrain the precursor environment of flares (active region filaments) and CMEs (filament cavities). Such measurements are critically important to understanding the formation, structure, destabilization, and eruption of such structures and their role in CMEs and interplanetary flux ropes. **The exploitation of free-free emission to determine the spatially-resolved temperature, density and magnetic fields in the quiet chromosphere, corona, and filaments in 3D** is possible only because of FASR's unique ability to perform high-resolution, high-dynamic-range imaging spectroscopy. Additional details may be found in the White Paper by Bastian et al. (2019b).

### 3 Technical Overview

The FASR concept presented here differs in key respects from previous versions. First, significant investments have been made in ground-based low-frequency arrays (<200 MHz): LOFAR, MWA, LWA, OVRO-LWA. A separate antenna subsystem (FASR-C) to observe frequencies <200 MHz is no longer a priority because arrays like OVRO-LWA will support science in this frequency band simultaneously with FASR. Second, the requirement for 1" imaging at a fiducial frequency of 20 GHz has been relaxed to 1.5" at 20 GHz, which significantly reduces the number of antennas  $N$  required, the area they occupy, and the size of the correlator, which scales as  $N^2$ . This descope has been adopted for three reasons. First, it enables FASR to be deployed at Owens Valley where the core EOVSAs array has already been deployed. Second, there is significant infrastructure and support available at Owens Valley. Third, it ensures that the cost of FASR remains modest. The previous costing exercise (see below) put the cost of FASR at approximately \$68M (FY2010), near the cusp between NSF's new midscale infrastructure program and the Major Research Equipment and Facilities Construction (MREFC) line. The MREFC line is probably not a realistic funding vehicle for FASR. It would require significant investments in development and implementation planning and would likely require many years of effort. FASR has always been conceived as a midscale project, one that could be implemented more nimbly and, if need be, in phases. While the angular resolution is slightly decreased by this choice, it is an excellent match to ALMA mm observations and is sufficient to address the key science objectives outlined in §2.

FASR's design is driven by several factors. First, the instrument must meet the science specifications derived from the key science objectives outlined in §2. Second, it must meet the needs of the large and diverse scientific community. Since most users will not be radio interferometrists, they should not bear the burden of data calibration and reduction. As a result, these functions must be performed by automatic data processing that delivers high-level, fully calibrated data products to a broad user community. Third, it is imperative to control the long-term operating and maintenance costs. Finally, it is important to design an expandable/upgradable system in order to respond flexibly to opportunities presented by new resources, new technologies, and/or new science objectives in the future. Invaluable experience on all the aspects above has been gained through the successful construction and operation of EOVSAs, which has already been engaging a much broader community to exploit the new radio imaging spectroscopic data than ever before.

### 3.1 Instrument Specifications

The science objectives outlined in §2 flow down to the high-level science and technical specifications summarized in the Table 1. FASR is designed to perform Fourier synthesis imaging using well-established interferometric techniques. For an array of  $N$  antennas there are  $\sim N^2/2$  independent antenna pairs, each of which measures a single Fourier component, or complex *visibility*, of the Sun's radio brightness distribution at a given frequency, time, and spatial frequency. The ensemble of antenna pairs, or *antenna baselines*, therefore measures many Fourier components. Fourier inversion of the visibility measurements yields an image of the Sun's radio brightness at a given frequency, time, and polarization. Deconvolution techniques are then used to remove the effects of the *point spread function*, the response of the instrument to a point source.

FASR observations will cover the frequency range of 200 MHz to 20 GHz (wavelengths from 1.5 cm to 1.5 m) using two separate arrays of antennas, denoted FASR A and FASR B. Each array provides frequency coverage over roughly a decade of bandwidth:  $\sim 2$ -20 GHz (FASR A);  $\sim 0.2$ -2.5 GHz (FASR B). The number, type, and configuration of the antennas in each array are chosen to address the key science objectives summarized in §2. The antennas will be distributed over an area with a diameter  $\sim 3$  km, providing an angular resolution of  $1.5''$  at 20 GHz over an hour angle range of at least  $\pm 3$  hr. The angular

Angular resolution	$30/\sqrt{\text{GHz}}$ arcsec
Frequency range	200 MHz – 20 GHz
Number data channels	2 (dual polarization)
Frequency bandwidth	1 GHz per channel
Frequency resolution	Instrumental: 125 kHz Scientific: min(1%, 5 MHz)
Time resolution	$\sim 0.4$ s (full spectrum sweep) 20 ms (dwell)
Polarization	Full Stokes (IQUV)
Number antennas deployed	<b>A</b> (2-20 GHz): $\sim 64$ <b>B</b> (0.2-2 GHz): $\sim 48$
Size antennas	<b>A</b> (2-20 GHz): 2 m <b>B</b> (0.2-2 GHz): 6 m
Array size	3 km linear size
Absolute positions	1 arcsec
Absolute flux calibration	$<10\%$

resolution scales linearly with wavelength from this fiducial value and is sufficient to resolve typical solar radio sources as well as being well matched to the capabilities of existing and planned space missions. The antenna size for each sub-array is determined by the competing needs of full disk imaging on the one hand, and sufficient sensitivity to calibrate the instrument against sidereal sources on the other.

## 4 Technology Drivers

FASR exploits radio astronomical techniques that have a substantial heritage, namely, Fourier synthesis imaging and image deconvolution. Moreover, a FASR pathfinder array has already been deployed (EOVSA) that leveraged the previous FASR design effort and has demonstrated the fast-tuning technology as well as the approach taken to calibration and imaging, thereby retiring

technical elements that were previously regarded as carrying minor to moderate risk. From a technical standpoint, there are no “tall poles” barring the way or significant risk elements. We recognize, however, that the FASR design needs to be re-optimized considering the continued advances in technology that offer improved solutions to well-understood problems: e.g., better ultra-wideband feeds and higher performance approaches to digital signal processing for a given price point are available.

## 5 Project Organization and Status

Previously, the FASR project was conceived as a consortium of university partners and national observatories under the management of Associated Universities, Inc. Lack of funding brought FASR development to an end aside from efforts leading to EOVSa, as well as narrowing of the consortium to implement EOVSa. Our multiple proposals to NSF to provide funding for continuing development and implementation of FASR have not been successful despite the multiple decadal endorsements. This is in large part a result of the fact that, until this year, NSF had no specific mechanism to fund mid-scale infrastructure. A bright spot, however, has been the EOVSa pathfinder project for which NJIT leveraged earlier development to successfully construct a 13-antenna array that began operating in early 2017. It is producing superb demonstrator flare science (see example in §2) and has served as the impetus for developing spectral analysis theory and for designing analysis tools to support dynamic radio imaging spectroscopy [e.g., 20,33].

FASR as a project requires a restart, both in terms of re-establishing the university-led partnership and in terms of developing a detailed design and implementation plan.

## 6 Project Schedule

We are not in a position to provide a detailed schedule, although as noted earlier the technology is ready to support completion in time for the next solar maximum (2025) given a new start by 2021. As noted, the project needs to update the design, prototype subsystems that take advantage of recent technological advances, and develop a detailed project execution plan, which will include cost and schedule. We presented a detailed plan to the Astro2010 decadal based on 5 years of planning funded by NSF. We went through a CATE evaluation and the project was described as “doable now” and was given a number two ranking by the RMS panel, as a midscale program with a total cost of approximately \$68M, and a schedule of 5 years. However, as noted, there was no budgetary mechanism to move the project forward within NSF at that time. We believe that a detailed implementation plan for the descoped FASR described here could be developed on a time scale of 2 years with deployment of the instrument requiring 4 years.

## 7 Cost Estimate

The FASR instrument concept has evolved over the years and has gone through several different costing exercises. The most comprehensive costing exercise was the result of the FASR team’s response to the NSF ATM Mid-Sized Infrastructure (MSI) Opportunity a decade ago for which detailed costs were developed for a reference instrument. The proposal was prepared by the FASR team, with task leaders providing detailed cost estimates for each element of the work breakdown

structure. Both the budget and schedule were reviewed by an external “red team”. This subsequently served as the basis for the cost estimate conveyed to Astro2010, which evaluated the project using the CATE process (analogous to the TRACE process). In addition, costs were analyzed for operations and maintenance of FASR, including a data management plan. These are no longer relevant.

Here, we can only provide a rough estimate (SWAG) of the rescoped FASR concept based on scaling up EOVSAs, recognizing that detailed costing is required as part of the (re-)development effort. Table 3 provides rough cost estimates for FASR A and FASR B in k\$, assuming a four-year project. The costs of the latter are more uncertain because the site has not been selected and because a complete system has not been prototyped. The numbers are based on scaling an NSF MSIP proposal that would have sited a prototype array in the radio quiet zone in Green Bank, WV. We are aware that overall costs depend on a number of factors, including the duration of the project, whether the two antenna subsystems (FASR A and B) are co-located, and whether they are constructed as part of a single project or as two largely independent efforts.

We note that the project cost presented to Astro2010 was \$53M plus contingency and management fees for a total of \$68M. We do not include contingency and fees here and so the comparison should be made with the \$53M figure; i.e., the descoped version of the instrument will cost approximately half the full original: ~\$26M. **FASR is a mid-scale ground-based project.**

<b>WBS no.</b>	<b>Task name</b>	<b>FASR A (64 antennas)</b>	<b>FASR B (32 antennas)</b>
<b>1.01</b>	<b>Project office</b>	3000 <sup>a</sup>	2000
<b>1.02</b>	<b>Site development</b>	1140	2100
<b>1.03</b>	<b>Antennas</b>	2560 <sup>b</sup>	6800
<b>1.04</b>	<b>Analog systems</b>	3550	600
<b>1.05</b>	<b>Digital systems</b>	380	1000
<b>1.06</b>	<b>Software and computing systems (SW&amp;C)</b>	1500 <sup>c</sup>	1000
<b>1.07</b>	<b>Systems engineering and integration (SE&amp;I)</b>	1500	1000
<b>1.08</b>	<b>Science, education and public outreach (S/EPO)</b>	300	-
		13930	12400

<sup>a</sup> Project office costs depend on a number of factors, including the duration of the project, whether the two antenna subsystems are co-located, and whether they are constructed as part of a single project or as two largely independent efforts.

<sup>b</sup> Antenna costs are based on vendor quotes for small numbers. The numbers likely over-estimate, perhaps significantly, the actual cost for the proposed number of FASR A and B antennas. In addition, for FASR B, there are ongoing development efforts to substantially decrease the cost of 5-6m antennas from which the project will benefit.

<sup>c</sup> Software and computing costs reflect the fact that EOVSAs has developed robust data calibration and analysis algorithms and associated software.

Table 1

Key Science Objectives	Science Goals	Measurement Goals	Observables	Emission Mechanism	Measurement Requirements <sup>1</sup>						
					Res'n	$\nu$	$\Delta\nu/\nu$	$D$	$\Delta T_b$	$\Delta\tau$	
<b>O1: The nature and evolution of coronal magnetic fields</b>	A: Coronal magnetography of active regions	Strong magnetic fields (>150 G)	a: Active region multi- $\nu$ $T_b$ maps	Gyroresonance	~1"	1-18	.01	3000	1000	1800	
	B: Coronal magnetography of the quiet Sun	LOS magnetic fields	b: Full-Sun multi- $\nu$ $T_b$ maps	Free-free	3"	1-21	.01	1000	300	1800	
	C: Magnetic connectivity of the corona to the heliosphere	Coronal field and topology	1a, 1b	See above	See above	-	-	-	-	-	-
			c: Active region multi- $\nu$ poln maps	Mode-coupling depolarization surface	~1"	1-21	.01	1000	1000	1800	
<b>O2: The physics of flares</b>	A: Magnetic energy storage	Preflare magnetography	d: dm- $\lambda$ , and m- $\lambda$ type III bursts	Plasma	20"	0.05-3	.01	1000	10 <sup>5</sup>	0.01	
	B: Magnetic energy release	Emission from upward and downward accelerated electrons	1a, 1b, 1c	See above	-	-	-	-	-	-	
			a: Flare multi- $\nu$ $T_b$ maps	Gyrosynchrotron	~1"	1-21	.01	10 <sup>4</sup>	10 <sup>5</sup>	1	
	C: Electron acceleration and transport	Electron distribution function	Electron distribution function	b: dm- $\lambda$ type III and reverse-slope bursts	Plasma	20"	0.3-3	.003	1000	10 <sup>5</sup>	0.01
<b>O3: Drivers of space weather</b>	A: Initiation and acceleration of CMEs	CME properties	c: Flare multi- $\nu$ $T_b$ maps	Gyrosynchrotron	~1"	1-21	.03	10 <sup>4</sup>	10 <sup>5</sup>	0.1	
	B: Origin and propagation of coronal shocks	Imaging of shocks, waves, and drivers	a: Full-Sun thermal and nonthermal dynamics	Free-free, Gyrosynchrotron	3"	0.3-18	.03	10 <sup>4</sup>	10 <sup>4</sup>	10	
			b: CME multi- $\nu$ nonthermal imaging	Synchrotron	60"	0.05-3	.03	1000	10 <sup>5</sup>	60	
	C: Origin of solar energetic particles	Spectral drift signature of emission	Imaging of shocks	c: CME multi- $\nu$ thermal imaging	Free-free	20"	0.3-3	.03	1000	1000	600
d: Coronal type II radio bursts				Plasma	120"	0.05-0.2	.01	100	10 <sup>4</sup>	10 <sup>4</sup>	0.1
<b>O4: Physics of the quiet solar atmosphere</b>	A: Thermal structure of the solar atmosphere	3D $T_e$ , $T_{th}$ , $B$ of the atmosphere	e: Imaging of Moreton waves	Free-free	3"	3-21	.03	10 <sup>4</sup>	1000	10	
	B: Coronal and chromospheric heating	Constraints on heating mechanisms	f: Imaging of prominence eruptions	Free-free, Gyrosynchrotron	~1"	1-21	.03	1000	300	10	
			3d, 3f	See above	-	-	-	-	-	-	
	C: Connectivity of atmosphere to heliosphere	3D mapping of coronal holes	3D $T_e$ , $T_{th}$ , $B$ of the atmosphere	h: type IV bursts	Plasma, Gyrosynchrotron	20"	0.05-3	.01	1000	10 <sup>5</sup>	10
			1a, 1b	See above	-	-	-	-	-	-	
			a: Full-Sun dm- $\lambda$ multi- $\nu$ $T_b$ maps	Free-free	20"	0.3-3	.03	1000	300	1800	
			1a	See above	-	-	-	-	-	-	
			b: Dynamical mapping of chromosphere and corona	Free-free	3"	0.3-21	.03	1000	300	1	
			1b, 4a	See above	-	-	-	-	-	-	

<sup>1</sup>Res'n = spatial resolution,  $\nu$  = frequency range (GHz),  $\Delta\nu/\nu$  = frequency resolution,  $D$  = dynamic range,  $\Delta T_b$  = brightness temperature sensitivity (K),  $\Delta\tau$  = time resolution (s)

## References

- [1] Aschwanden, M. J., Benz, A. O. 1997. Electron Densities in Solar Flare Loops, Chromospheric Evaporation Upflows, and Acceleration Sites. *The Astrophysical Journal* 480, 825-839.
- [2] Bastian, T. S., Benz, A. O., Gary, D. E. 1998. Radio Emission from Solar Flares. *Annual Review of Astronomy and Astrophysics* 36, 131-188.
- [3] Bastian, T. S., Pick, M., Kerdraon, A., Maia, D., Vourlidis, A. 2001. The Coronal Mass Ejection of 1998 April 20: Direct Imaging at Radio Wavelengths. *The Astrophysical Journal* 558, L65-L69.
- [4] Benz, A. O. 1994. Observations of fragmented energy release. *Space Science Reviews* 68, 135-147
- [5] Benz, A. O., Saint-Hilaire, P., Vilmer, N. 2002. Location of narrowband spikes in solar flares. *Astronomy and Astrophysics* 383, 678-684.
- [6] Bogod, V. M., Yasnov, L. V. 2016. Determination of the Structure of the Coronal Magnetic Field Using Microwave Polarization Measurements. *Solar Physics* 291, 3317-3328.
- [7] Brosius, J. W., White, S. M. 2006. Radio Measurements of the Height of Strong Coronal Magnetic Fields Above Sunspots at the Solar Limb. *The Astrophysical Journal* 641, L69-L72.
- [8] Chen, B., Bastian, T. S., White, S. M., Gary, D. E., Perley, R., Rupen, M., Carlson, B. 2013. Tracing Electron Beams in the Sun's Corona with Radio Dynamic Imaging Spectroscopy. *The Astrophysical Journal* 763, L21.
- [9] Chen, B., Bastian, T. S., Shen, C., Gary, D. E., Krucker, S., Glesener, L. 2015. Particle acceleration by a solar flare termination shock. *Science* 350, 1238-1242.
- [10] Chen, B., Yu, S., Battaglia, M., Farid, S., Savcheva, A., Reeves, K. K., Krucker, S., Bastian, T. S., Guo, F., Tassev, S. 2018. Magnetic Reconnection Null Points as the Origin of Semirelativistic Electron Beams in a Solar Jet. *The Astrophysical Journal* 866, 62.
- [11] De Rosa, M. L., and 18 colleagues 2009. A Critical Assessment of Nonlinear Force-Free Field Modeling of the Solar Corona for Active Region 10953. *The Astrophysical Journal* 696, 1780-1791.
- [12] Drake, J. F., Swisdak, M., Cassak, P. A., Phan, T. D. 2014. On the 3-D structure and dissipation of reconnection-driven flow bursts. *Geophysical Research Letters* 41, 3710-3716.
- [13] Fleishman, G. D., Nita, G. M., Kuroda, N., Jia, S., Tong, K., et al. 2018. Revealing the Evolution of Non-thermal Electrons in Solar Flares Using 3D Modeling. *The Astrophysical Journal* 859, 17.
- [14] Gary, D. E., Keller, C. U. 2004. *Solar and Space Weather Radiophysics - Current Status and Future Developments*. *Astrophysics and Space Science Library* 314.
- [15] Gary, D. E., Fleishman, G. D., Nita, G. M. 2013. Magnetography of Solar Flaring Loops with Microwave Imaging Spectropolarimetry. *Solar Physics* 288, 549-565.
- [16] Gary, D. E., and 10 colleagues 2018. Microwave and Hard X-Ray Observations of the 2017 September 10 Solar Limb Flare. *The Astrophysical Journal* 863, 83.
- [17] Ishikawa, S.-N., Glesener, L., Krucker, S., Christe, S., Buitrago-Casas, et al. 2017. Detection of nanoflare-heated plasma in the solar corona by the FOXSI-2 sounding rocket. *Nature Astronomy* 1,
- [18] Lanzerotti, L. 2004, in *Solar and Space Weather Radiophysics*, eds. D. E. Gary and C. Keller, Springer/Kluwer, *Astrophysics and Space Science Library*, v. 314

- [19] Lee, C. O., and 10 colleagues 2018. Observations and Impacts of the 10 September 2017 Solar Events at Mars: An Overview and Synthesis of the Initial Results. *Geophysical Research Letters* 45, 8871
- [20] Lin, H., Kuhn, J. R., Coulter, R. 2004. Coronal Magnetic Field Measurements. *The Astrophysical Journal* 613, L177-L180.
- [21] Maia, D. J. F., Gama, R., Mercier, C., Pick, M. Kerdraon, A., Karlicky, M. 2007. The Radio-Coronal Mass Ejection Event on 2001 April 15, *The Astrophysical Journal* 660, 874-881
- [22] National Research Council 2001. *Astronomy and Astrophysics in the New Millennium*. Washington, DC, National Academies Press
- [23] National Research Council 2003. *From the Sun to the Earth - and Beyond: A Decadal Research Strategy in Solar and Space Physics*, Washington, DC, National Academies Press
- [24] National Research Council 2010. *New Worlds, New Horizons in Astronomy and Astrophysics*. Washington, DC, National Academies Press
- [25] National Research Council 2012. *Solar and Space Physics: A Science for a Technological Society*. Washington, DC, National Academies Press
- [26] Nita, G. M., Fleishman, G. D., Kuznetsov, A. A., Kontar, E. P., Gary, D. E. 2015. Three-dimensional Radio and X-Ray Modeling and Data Analysis Software: Revealing Flare Complexity. *The Astrophysical Journal* 799, 236.
- [27] Petrosian, V. 2016. Particle Acceleration in Solar Flares and Associated CME Shocks. *The Astrophysical Journal*, 830, 28
- [28] Rahman, M. M., McCauley, P. I., Cairns, I. H. 2019. On the Relative Brightness of Coronal Holes at Low Frequencies. *Solar Physics* 294, 7.
- [29] Seaton, D. B., Darnel, J. M. 2018. Observations of an Eruptive Solar Flare in the Extended EUV Solar Corona. *The Astrophysical Journal* 852, L9.
- [30] Sharma, R., Oberoi, D., Arjunwadkar, M. 2018. Quantifying Weak Nonthermal Solar Radio Emission at Low Radio Frequencies. *The Astrophysical Journal* 852, 69.
- [31] Shibata, K., Magara, T. 2011, *Solar Flares: Magnetohydrodynamic Processes*. *Living Reviews in Solar Physics*, 8, 6
- [32] van Ballegoijen, A. A., Asgari-Targhi, M., Cranmer, S. R., DeLuca, E. E. 2011. Heating of the Solar Chromosphere and Corona by Alfvén Wave Turbulence. *The Astrophysical Journal* 736, 3.
- [33] White, S. M., Kundu, M. R. 1997. Radio Observations of Gyroresonance Emission from Coronal Magnetic Fields. *Solar Physics* 174, 31-52.
- [34] White, S. M. 2004. Coronal Magnetic Field Measurements Through Gyroresonance Emission. *Astrophysics and Space Science Library* 314, 89.
- [35] White, S. M., and Thompson, B. J. 2005. High-Cadence Radio Observations of an EIT Wave, *ApJ* 620, L63
- [36] Wright, P. J., Hannah, I. G., Grefenstette, B. W., Glesener, L., Krucker, S., et al. 2017. Microflare Heating of a Solar Active Region Observed with NuSTAR, Hinode/XRT, and SDO/AIA. *The Astrophysical Journal* 844, 132.

**White Papers Cited**

Airapetian, V., and 83 co-authors 2019, Reconstructing Extreme Space Weather from Planetary Hosted Stars, *Astro2020: Decadal Survey on Astronomy and Astrophysics*, science white papers, no. 564; *Bulletin of the American Astronomical Society*, Vol. 51, Issue 3, id. 564

Bastian, T. S. and 8 co-authors 2019, Diagnostics of Space Weather Drivers Enabled by Radio Observations, *Astro2020: Decadal Survey on Astronomy and Astrophysics*, science white papers, no. 323; *Bulletin of the American Astronomical Society*, Vol. 51, Issue 3, id. 323

Bastian, T. S., and 7 co-authors 2019, Radio, Millimeter, and Sub-millimeter Observations of the Quiet Sun, *Astro2020: Decadal Survey on Astronomy and Astrophysics*, science white papers, no. 493; *Bulletin of the American Astronomical Society*, Vol. 51, Issue 3, id. 493

Chen, B., and 11 co-authors 2019, Probing Magnetic Reconnection in Solar Flares: New Perspectives from Radio Dynamic Imaging Spectroscopy, *Astro2020: Decadal Survey on Astronomy and Astrophysics*, science white papers, no. 507; *Bulletin of the American Astronomical Society*, Vol. 51, Issue 3, id. 507

Fleishman, G., and 8 co-authors 2019, Solar Coronal Magnetic Fields: Quantitative Measurements at Radio Wavelengths, *Astro2020: Decadal Survey on Astronomy and Astrophysics*, science white papers, no. 426; *Bulletin of the American Astronomical Society*, Vol. 51, Issue 3, id. 426

Gary, G., and 7 co-authors 2019, Particle Acceleration and Transport, New Perspectives from Radio, X-ray, and Gamma-Ray Observations, *Astro2020: Decadal Survey on Astronomy and Astrophysics*, science white papers, no. 371; *Bulletin of the American Astronomical Society*, Vol. 51, Issue 3, id. 371

Osten, R., and 15 co-authors 2019, Advancing Understanding of Star-Planet Ecosystems in the Next Decade: the Radio Wavelength Perspective, *Astro2020: Decadal Survey on Astronomy and Astrophysics*, science white papers, no. 434; *Bulletin of the American Astronomical Society*, Vol. 51, Issue 3, id. 434